APPLICATIONS PAPER

Ground-Level Ozone Concentration and Landscape Patterns in China's Urban Areas

Jiayi Li and Xin Huang

Abstract

We monitored the spatio-temporal distribution of urban population-weighted ozone for 2014–2017 to investigate ground-level pollution in China. During the study period, the national average was 88.68±10.4 μg/m³ for O3-8h, and 5.27% of the days that exceed the 160 μg/m³ standard. Pollution hotspots in the Tibetan Plateau are mainly attributed to natural factors, while those in the North China Plain (NCP), Yangtze River Delta (YRD), and Pearl River Delta (PRD) are more closely related to anthropogenic activities. The results indicate that the ozone pollution and its correlations with the landscape are influenced by the ozone regime and climatic factors. In the Yangtze Plain and to its south, pollution in the ozone episodes is related to both population size and heterogeneity. For the Yangtze Plain and its southern urban areas in transitional ozone regimes, sprawl, contiguity, compactness, and the size of the urban area also facilitate the accumulation of pollution.

Introduction

During the last few decades in China, the rapid industrialization and urbanization have been accompanied by elevated air pollution at a national scale. Recently, much attention has been paid to ground-level ozone, which is an important risk factor for both human health and vegetation (Feng *et al.*, 2015; Lefohn *et al.*, 2017; Lelieveld *et al.*, 2015; Liu *et al.*, 2018). It has been reported that, in summer, most of the developed and populated city clusters in China, such as the Yangtze River Delta (YRD) (Shao *et al.*, 2016; Shu *et al.*, 2016), the Pearl River Delta (PRD) (GPEMC, 2017), and the Beijing-Tianjin-Hebei (BTH) region (Wang *et al.*, 2017), are facing serious photochemical pollution. As a ground-level secondary pollutant, in addition to the downward transport of stratospheric air and horizontal wind transport, ground-level ozone is generated through photochemical reactions, which is a process that requires the presence of sunlight and the participation of emitted precursors. With an abundant diversity of precursors in the different ozone formation regimes and the complicated synoptic meteorological conditions in China, it is a challenging task to analyze the influence of anthropogenic activities on urban ozone pollution.

Since the mid-2000s, several studies have been made of surface photochemical pollution in populated areas in China, including model simulations (Ou *et al.*, 2016), satellite data analyses (Huang *et al.*, 2013; Jin *et al.*, 2017; Jin and Holloway, 2015), and field experiments (Jia *et al.*, 2016; Shu *et al.*, 2016). Due to the coarse spatial resolution of the data, the observation of ozone in the first two approaches has mainly focused on global- or regional-scale studies (Li *et al.*, 2017; Liu *et al.*, 2018). Meanwhile, the most recent satellite remote sensing data can provide us with the precursor distribution at a finer spatial resolution (Jin *et al.*, 2017), which can be used to estimate the formation mode of ground-level ozone. On the other hand, some studies have focused on the dynamic differences between urban and rural sites, based on large cities (Jia *et al.*, 2016) or agglomerations (GPEMC, 2017), using field observations from several ground stations. However, the conclusions from these studies may not be comprehensive or may even be contradictory, partly because of the limitations of the regional climate conditions, the geographical locations, and the development levels. For instance, Huang *et al.* (2013) argued that tropospheric ozone was insensitive to urbanization in three urban agglomerations in east China, while Li *et al.* (2017) suggested that the intensified urban heat island phenomenon during urbanization aggravated the ozone pollution and the emission of its precursors in the YRD urban cluster. It is also notable that relatively small cities in China account for a substantial proportion of the population, and the ground-level ozone situation in these areas should thus be monitored. Since 2013, a national-scale network, which tracks and regulates the Environmental Protection Agency (EPA)'s six criteria pollutants (including ground-level ozone), has been gradually constructed by the Chinese Ministry of Ecology and Environment (MEE), to facilitate the monitoring of near real-time in-situ, ground-level ozone. This context provides us with an opportunity to investigate the spatio-temporal characteristics of urban ground-level ozone and its relationships with urbanization in multiple cities.

Urban landscape indicators are metrics that can be used to reveal linkages between urbanization and environmental consequences (Bai *et al.*, 2011; Fang *et al.*, 2016; Pontius and Gilmore, 2017). The built environment in urban landscapes, relating to the surrounding site environment, exhibits unique radiative, thermal, moisture, and aerodynamic properties (Frank and Engelke, 2005; Oke, 1982). The demographic distribution in urban landscapes, influencing the metabolism of the surrounding districts, also portrays the magnitude and extent of human activity (Zhu *et al.*, 2015). In this context, a number of studies have reported that urban landscapes have a significant impact on local air pollution, such as nitrogen oxides (NO_x) (Bechle *et al.*, 2011; Larkin *et al.*, 2016), sulfur dioxide (SO_2) (Zou *et al.*, 2007), and fine particles with a diameter of 2.5 μm or less ($PM_{2.5}$) (Larkin *et al.*, 2016; Li *et al.*, 2016). In recent years, the effects of urban planning and spatial optimization methods on ground-level ozone concentration have also been investigated. For instance, taking US urban areas as the study region, population centrality has

Jiayi Li is with the School of Remote Sensing and Information Engineering, Wuhan University, P.R. China, 129 Luoyu Road, Wuhan, Hubei, 430079 P.R. China,

Xin Huang is with the School of Remote Sensing and Information Engineering, Wuhan University, Wuhan 430079, PR China; and the State Key Laboratory of Information Engineering in Surveying, Mapping and Remote Sensing, Wuhan University, Wuhan 430079, PR China, 129 Luoyu Road, Wuhan, Hubei, 430079 P.R. China, (xhuang@whu.edu.cn).

Photogrammetric Engineering & Remote Sensing
Vol. 85, No. 2, February 2019, pp. 145–152.
0099-1112/18/145–152

doi: 10.14358/PERS.85.2.145

been associated with lower concentrations of ground-level ozone (Clark *et al.*, 2011; McCarty and Kaza, 2015), while the urban sprawl level of large metropolitan regions has been positively linked to a greater number of ozone exceedances (Stone, 2008). It is therefore remarkable that so few studies have engaged in the task of estimating the influence of urban form on ground-level ozone. Furthermore, very few studies have paid attention to the distinct functions of the urban form under different ozone formation regimes, especially in China. Hence, there is an urgent need to investigate the relationship between the urban landscape and ground-level ozone pollution, considering the ozone formation regimes, for the different cities in the diverse climate zones of China.

In this study, we built one of the first long-term urban ground-level ozone datasets for China, which includes the ground-level ozone concentration (referred to as "ozone concentration" hereafter) measured during three years of continuous monitoring in the urban areas of all the prefecture-level (or above) cities in China. About 1,563 monitoring stations in 339 cities were operating between June 2014 and May 2017. In this paper, an overview of the spatio-temporal variations of the urban ozone pollution is documented. In the different ozone formation regimes and climate zones, the relationships between several typical urban characteristics (including the built environment and demographic factors) and ozone concentration over the study period are investigated. By studying this extensive dataset, our understanding of the urban ozone pollution at a fine spatio-temporal resolution should be enhanced. The findings of this paper will provide valuable advice for the development of pollution reduction policies for high-pollution days and for the improvement of urban air quality from the perspective of urban landscape design, accounting for the climate conditions and the ozone formation regimes throughout China.

Materials and Methods

Figure 1 shows the framework of the method used to estimate the urban ozone status and reveal its relationship with urban characteristics. The four steps marked in Figure 1 are described in detail in the following.

Study Region and Urban Areas

All the prefecture-level cities in China, except for those in some autonomous regions, were included in this study. The ~30 m gridded summary of national land cover (the China Land Use/Cover Dataset [CLUD], which includes water bodies, built-up land, etc.) for the year circa 2015 (Liu *et al.*, 2014), an elevation dataset (URL: *http://earthexplorer.usgs.gov/*), and the administrative boundaries (URL: *http://www.gadm.org*) were utilized for the urban area extraction. Details of the urban boundary calculation procedure are shown in Figure 2. Pixels of water bodies or those pixels with elevations exceeding the highest point in the urban area by 50 m were excluded from this analysis.

Climate Zones and Ozone Formation Regimes

According to the Köppen-Geiger climate classification system (Rubel and Kottek, 2010), the mainland of China can be divided into five climate zones by the different climatic conditions (i.e., rainfall and temperature, which are important natural environmental factors related to ozone). EW stands for equatorial climate and warm and fully humid temperate climate; W stands for warm temperate climate with dry winter; A stands for the climate of arid steppe and desert; S stands for snow climate with dry winter; and TS, at the Qinghai-Tibet Plateau, stands for tundra climate and snow climate with cool summer and cold winter.

The Ozone Monitoring Instrument (OMI) onboard NASA's Earth Observing System Aura satellite can provide us with the major proxies of the ozone precursors, including nitrogen dioxide (NO_2) and formaldehyde (HCHO) (Ziemke *et al.*, 2006), which are widely used for determining the ozone formation regime. For the study period, the concentration of monthly NO_2 was obtained with a resolution of 0.125° (DOMINO–OMI–NO_2v2) and an uncertainty of 1×10^{15} mol/cm^2±25%, and that of the monthly HCHO was acquired with a resolution of 0.25° (BIRA–OMI–HCHOv14) and an overall error of 7×10^{15} mol/cm^2 (De Smedt *et al.*, 2015). Firstly, following the criteria applied in East Asia in a previous study (Jin *et al.*, 2017), the ozone regime for each grid cell was classified as either null, a volatile organic compound (VOC)-limited regime, a NO_x-limited regime, or a transitional regime. A grid cell where the average concentration of NO_2 was less than 2.5×10^{15} mol/cm^2 was set as null and regarded as an insensitive area for anthropogenic activities. We then recorded the percentage of the ozone regime classes within each urban area. For each urban area whose dominant regime was not null, it was assigned as the regime class with the highest percentage when this percentage was larger than 50%; otherwise, it was regarded as a mixed region.

Population-Weighted Ground-Level Ozone Concentration Estimation

Since 2013, a national network of 1,563 monitoring stations has been gradually established by the MEE. In this network, at least one station is located in each prefecture-level city of China. Quality control of the utilized data in this study (from 01 June 2014, to 31 May 2017) was based on the National Ambient Air Quality Standards (NAAQS) (GB 3095–2012) (Chinese MEP, 2012).

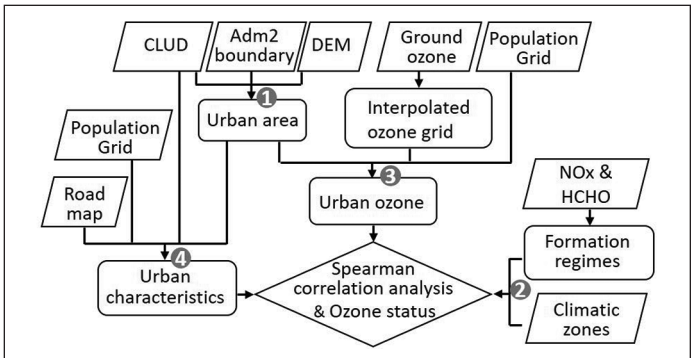

Figure 1. Framework of the method utilized in this study.

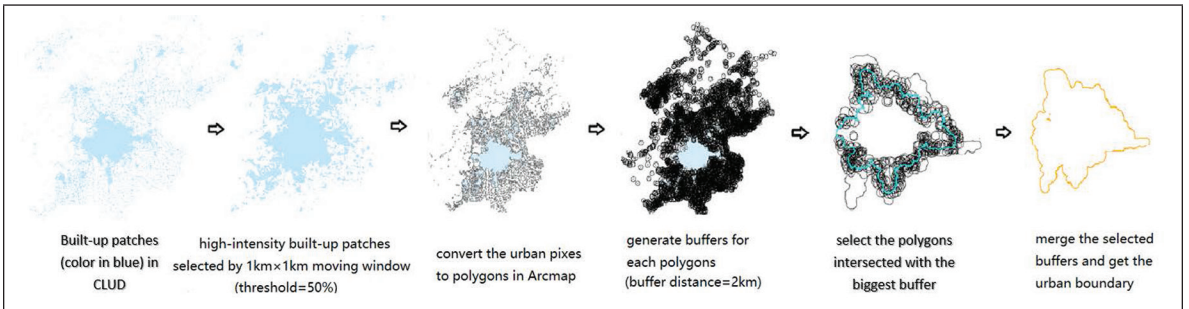

Figure 2. Urban boundary calculation procedure for each city of China, taking Beijing as an example.

As suggested by Clark *et al.* (2011), the population-weighted (PW) ozone concentration for each urban area was estimated as follows. Firstly, for each hour, the available concentrations from the 12 nearest monitoring stations were fed into the inverse distance weighting based spatial interpolation method to simulate the ozone grid. We estimated the model performance by comparing the modeled results with observations from 1,241 monitoring sites of urban areas in China. In general, the simulated ozone agreed well with the observations, with correlation coefficients greater than 0.99 (p <0.001). We then used the latest gridded population dataset (POP) (1-km spatial resolution, year 2010), which was obtained from the Data Center for Resources and Environmental Sciences (RESDC) of the Chinese Academy of Sciences (Fu *et al.*, 2014). PW ozone was then calculated as follows:

$$\mathrm{PW-ozone} = \sum_{i=1}^{n}(ozone_i \times POP_i) / \sum_{i=1}^{n} POP_i \quad (1)$$

For the urban area of each city, PM_i and $ozone_i$ are the interpolated concentration and the population within each prefecture, respectively, in each 1 km grid-cell center i, where n is the number of 1 km grid-cell centers within the current urban area. Finally, the annual dynamics for 2014–2017 were calculated, where June to the next May was regarded as one year. Considering the seasonal and diurnal factors, we calculated the daily, daytime, and nighttime average ozone concentrations, and O_3-8h, for all year round and the ozone episode periods, respectively.

Urban Characteristics

The spatial pattern of the built-up areas and population was used to understand and quantify the anthropogenic activity impact on the concentration of ozone (Figure 3). The built-up related metrics were extracted from the CLUD circa 2015 and the POP dataset circa 2010 (Fu *et al.*, 2014). Roads were extracted from Map World (URL: *http://www.tianditu.cn/*). Detailed descriptions of the urban landscape metrics are provided in Table 2, and the descriptive statistics are listed in Table 3.

Results

The pollution situations of the 339 urban areas in the mainland of China, grouped by the five climate zones, were analyzed. Both the spatio-temporal distribution and the seasonal and diurnal variation of the pollution in China were also analyzed. Spearman's rank correlation coefficients were then calculated to investigate the relationships between ozone pollution during the ozone season and the urban landscape metrics.

Overview and Spatial Distribution of Ozone Pollution in China

Figure 4 presents the spatial distribution of the triennial average concentrations of the 339 cities in China. Taking all the cities as a whole, the triennial average was 55.34 ±7.77 μg/m^3 for daily ozone and 88.68 ±10.41 μg/m^3 for O_3-8h over the study period. The triennial average O_3-8h concentration ranged from 60.75±33.50 μg/m^3 (Urumqi in the A climate zone) to 119.46±55.47 μg/m^3 (Weifang in the W climate zone). As can be seen in Figure 4, the highest average concentrations of all four metrics (i.e., daily average, daytime, nighttime, and O_3-8h) were found in the TS climate zone, the North China Plain (NCP) (in the W zone), and the YRD (in the EW zone). In the meantime, cities in the PRD (in the EW zone) also suffered from unignorable ozone pollution in both daytime and nighttime. Ozone pollution in the TS urban areas is less related to anthropogenic sources, as the ozone formation regimes of the

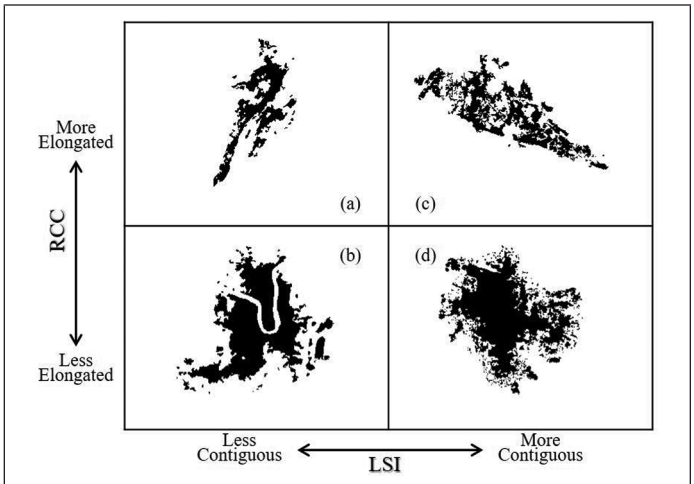

Figure 3. Elongation and contiguity of the built-up patches within the urban areas, illustrated by (a) Zunyi, in the EW climate zone (0.85, 9, and 88 for RCC, LSI, and the three-year average concentration of PW O3-8h, respectively); (b) Liuzhou in the EW climate zone (0.64, 8, 99); (c) Shiyan in the W climate zone (0.86, 17, 95); and (d) Changzhou in the W climate zone (0.55, 16, 125).

Table 1. Description of the urban landscape metrics.

Abbreviation	Full name	Formulation	Description
POPI	Population density intensity	mean(p)	POPI measures the mean value of population density within an urban area, where p stands for the population grid for each pixel.
POPV	Variation in population density	std(p)	POPV is an indirect indicator of urban sprawl, which indicates how low-density suburban areas contrast with high-density urban centers (Larkin *et al.*, 2016).
CA	Total area of built-up land	sum(b)	CA measures the urban extent, where b represents the built-up pixels.
NP	Number of built-up patches within the urban area	n	NP is proportional to the urban fragmentation level.
LSI	Landscape shape index	$0.25\times\mathrm{sum}(e)/A^{0.5}$	LSI measures the total length of all the edge segments related to a given urban patch to describe the continuity. e means the total length of edge in the urban area between the built-up class and the other land-cover types. A is the total area of the urban area.
RCC	Related circumscribing circle index	1-(sum(b))/A	RCC is an elongation measure for urban areas. A highly convoluted but narrow urban area will have a low RCC value, due to the relative compactness, yet a narrow and elongated urban area will have a high response.
DIST	Distance from urban area to the coast	d	DIST measures the distance from the urban area to the coast.
RD	Road density	sum(r)/sum(b)	RD is measured by dividing the total area of road by CA. r is the road pixels.

14 urban areas (Table 3, 14/15 = 93.3%) are assigned as null. Similar nocturnal ozone concentration results are seen in the high-altitude urban areas (Figure 4d).

Temporal Variation of Ozone Pollution in China

Fine weather with intense sunlight, high temperature, and low wind velocity is an ideal breeding ground for ozone episodes. In view of the diurnal variation, the lower ozone concentration during the nighttime can be explained by the low temperature, as well as dry deposition. As can be seen in Figure 5, for all the metrics except for nocturnal ozone, the W and S zones

Table 3. Number of urban areas assigned by the ozone formation regime criteria across the five climate zones.

	NOx-limited	Transitional	VOC-limited	Null	Mixed
EW	37	27	0	50	1
W	31	41	2	43	0
A	3	10	0	20	0
S	14	19	3	23	0
TS	1	0	0	14	0
China	86	97	5	150	1

Table 2. Descriptive statistics of the urban landscape metrics grouped by climate zones and ozone formation regimes.

		EW		W		A	S		China	
	Regime	NOx-limited	Transitional	NOx-limited	Transitional	Transitional	NOx-limited	Transitional	NOx-limited	Transitional
POPI	mean	6.00e+05	7.58e+05	1.41e+06	1.49e+06	1.46e+06	5.17e+05	2.83e+05	7.53e+05	8.51e+05
	IQR	4.8e+05	5.1e+05	1.4e+06	8.3e+05	4.5e+05	4.0e+05	1.8e+05	5.8e+05	6.7e+05
POPD*	mean	5.33e+02	4.06e+02	4.41e+02	4.32e+02	5.14e+02	4.93e+02	3.58e+02	4.93e+02	3.99e+02
	IQR	3.7e+02	2.4e+02	2.5e+02	2.3e+02	4.2e+02	3.6e+02	2.4e+02	3.5e+02	2.4e+02
POPV	mean	3.81e+03	2.94e+03	3.46e+03	3.43e+03	3.63e+03	3.71e+03	3.09e+03	3.67e+03	3.18e+03
	IQR	3.1e+03	1.7e+03	2.5e+03	2.2e+03	3.8e+03	2.3e+03	2.3e+03	2.4e+03	2.3e+03
CA	mean	9.99e+03	2.30e+04	2.98e+04	3.20e+04	3.41e+04	8.28e+03	5.28e+03	1.39e+04	1.98e+04
	IQR	3.9e+03	1.4e+04	3.9e+04	2.1e+04	3.3e+04	5.9e+03	2.5e+03	7.8e+03	1.4e+04
NP	mean	72.00	128.58	159.11	151.41	200.50	45.36	30.67	81.09	101.83
	IQR	44.3	104.0	212.5	65.8	259.0	29.0	26.0	63.5	103.5
LSI	mean	12.13	12.82	13.78	13.06	15.16	9.10	7.98	11.19	11.16
	IQR	3.4	5.3	10.0	4.5	11.0	2.8	4.6	5.2	4.5
RCC	mean	0.263	0.272	0.274	0.288	0.237	0.228	0.208	0.250	0.253
	IQR	0.116	0.104	0.101	0.148	0.055	0.111	0.060	0.097	0.124
DIST	mean	4.19e+03	4.52e+03	2.50e+03	3.83e+03	2.31e+03	3.10e+03	6.26e+03	3.29e+03	4.88e+03
	IQR	6.3e+03	7.7e+03	2.9e+03	4.7e+03	2.7e+03	3.3e+03	4.8e+03	4.5e+03	6.7e+03
RD	mean	0.121	0.131	0.125	0.116	0.108	0.099	0.106	0.113	0.116
	IQR	0.054	0.047	0.051	0.035	0.008	0.050	0.036	0.055	0.041

* POPD is the abbreviation for population density, and is equal to POPI divided by CA

Table 4. Non-attainment days and exceedance rates for the Grade II standard (160 μg/m_3) and Grade I standard (100 μg/m3) for each climate zone and China as a whole

N(e)*	EW		W		A		S		TS		China	
Grade standard	II	I	II	I	II	I	II	I	II	I	II	I
Jan.	6 (0.06)	734 (7.09)	8 (0.08)	521 (4.95)	0 (0.00)	66 (2.22)	0 (0.00)	10 (0.19)	0 (0.00)	36 (2.67)	14 (0.05)	1367 (4.48)
Feb.	14 (0.14)	2058 (21.05)	5 (0.05)	1494 (15.02)	1 (0.04)	115 (4.10)	0 (0.00)	152 (3.03)	2 (0.16)	193 (15.14)	22 (0.08)	4012 (13.92)
Mar.	32 (0.30)	2896 (27.37)	76 (0.71)	3975 (36.93)	7 (0.23)	850 (28.00)	37 (0.68)	1491 (27.47)	0 (0.00)	685 (49.64)	152 (0.49)	9897 (31.73)
Apr.	684 (6.68)	4776 (46.66)	614 (5.90)	6124 (58.81)	23 (0.78)	1722 (58.63)	192 (3.66)	2891 (55.06)	27 (2.02)	978 (73.26)	1540 (5.10)	16491 (54.66)
May	1512 (12.06)	6448 (51.44)	2374 (18.62)	8901 (69.80)	170 (4.73)	2467 (68.58)	1214 (18.88)	4330 (67.33)	51 (3.12)	1336 (81.71)	5321 (14.40)	23482 (63.55)
Jun.	872 (8.43)	3858 (37.28)	1888 (17.93)	5758 (54.68)	152 (5.12)	2115 (71.21)	772 (14.54)	3518 (66.25)	32 (2.37)	846 (62.67)	3716 (12.18)	16095 (52.75)
Jul.	761 (7.88)	3809 (39.43)	1424 (14.49)	5744 (58.45)	248 (8.95)	2150 (77.56)	702 (14.16)	3488 (70.38)	52 (4.13)	722 (57.30)	3187 (11.19)	15913 (55.88)
Aug.	882 (8.34)	4845 (45.79)	982 (9.12)	5776 (53.66)	70 (2.31)	1879 (61.89)	329 (6.06)	2742 (50.52)	4 (0.29)	715 (51.81)	2267 (7.27)	15957 (51.16)
Sep.	963 (9.63)	5132 (51.29)	816 (8.02)	4184 (41.10)	3 (0.10)	973 (33.89)	138 (2.69)	1513 (29.48)	0 (0.00)	290 (22.22)	1920 (6.51)	12092 (41.00)
Oct.	671 (6.27)	4873 (45.56)	432 (3.97)	2893 (26.59)	2 (0.07)	294 (9.58)	93 (1.69)	846 (15.42)	1 (0.07)	271 (19.43)	1199 (3.80)	9177 (29.11)
Nov.	23 (0.23)	963 (9.52)	13 (0.13)	607 (5.90)	0 (0.00)	37 (1.27)	0 (0.00)	58 (1.12)	0 (0.00)	51 (3.86)	36 (0.12)	1716 (5.75)
Dec.	7 (0.07)	597 (6.04)	6 (0.06)	393 (3.91)	0 (0.00)	34 (1.20)	0 (0.00)	8 (0.16)	0 (0.00)	28 (2.17)	13 (0.04)	1060 (3.64)
All	6427 (5.15)	40989 (32.85)	8638 (6.80)	46370 (36.53)	676 (1.89)	12702 (35.48)	3477 (5.43)	21047 (32.88)	169 (1.04)	6151 (37.79)	19387 (5.27)	127259 (34.60)
Ozone season	6345 (8.57)	33741 (45.56)	8530 (11.32)	39380 (52.26)	640 (5.17)	8611 (69.58)	3440 (9.05)	19328 (50.87)	135 (3.18)	2904 (68.41)	19090 (9.36)	103964 (50.96)

Note: N(e): N and e mean the number of non-attainment days and the exceedance rate (unit: %) for all cities in each zone

present the highest average concentrations, followed by the A, EW, and TS zones in the growing season (spring and summer), while the TS and EW zones show a higher concentration than the others in winter. For nocturnal ozone, the TS zone shows a higher concentration than the other regions. With regard to seasonality, significant variability can be seen, with the highest concentration in the growing season and the lowest in the winter. Taking China as a whole, all the ozone measurements are presented as the approximated unimodal distribution by season (see the green bars in Figure 5). Besides May as the most severe period for all the climate zones, the other seriously affected months are September in the EW zone and July for both the A and S zones. According to the NAAQS of China, the non-attainment days that exceeded the O_3-8h limit (i.e., 160 μg/m^3 for urban areas) for each zone are listed in Table 4. For O_3-8h, daily ozone, and daytime ozone, the most severe exceedance rates for the EW, W, and S climate zones are from March to October, while the most severe exceedance rates for the A zone are from May to July, and the most severe exceedance rates for the S zone are from May to August. The ozone

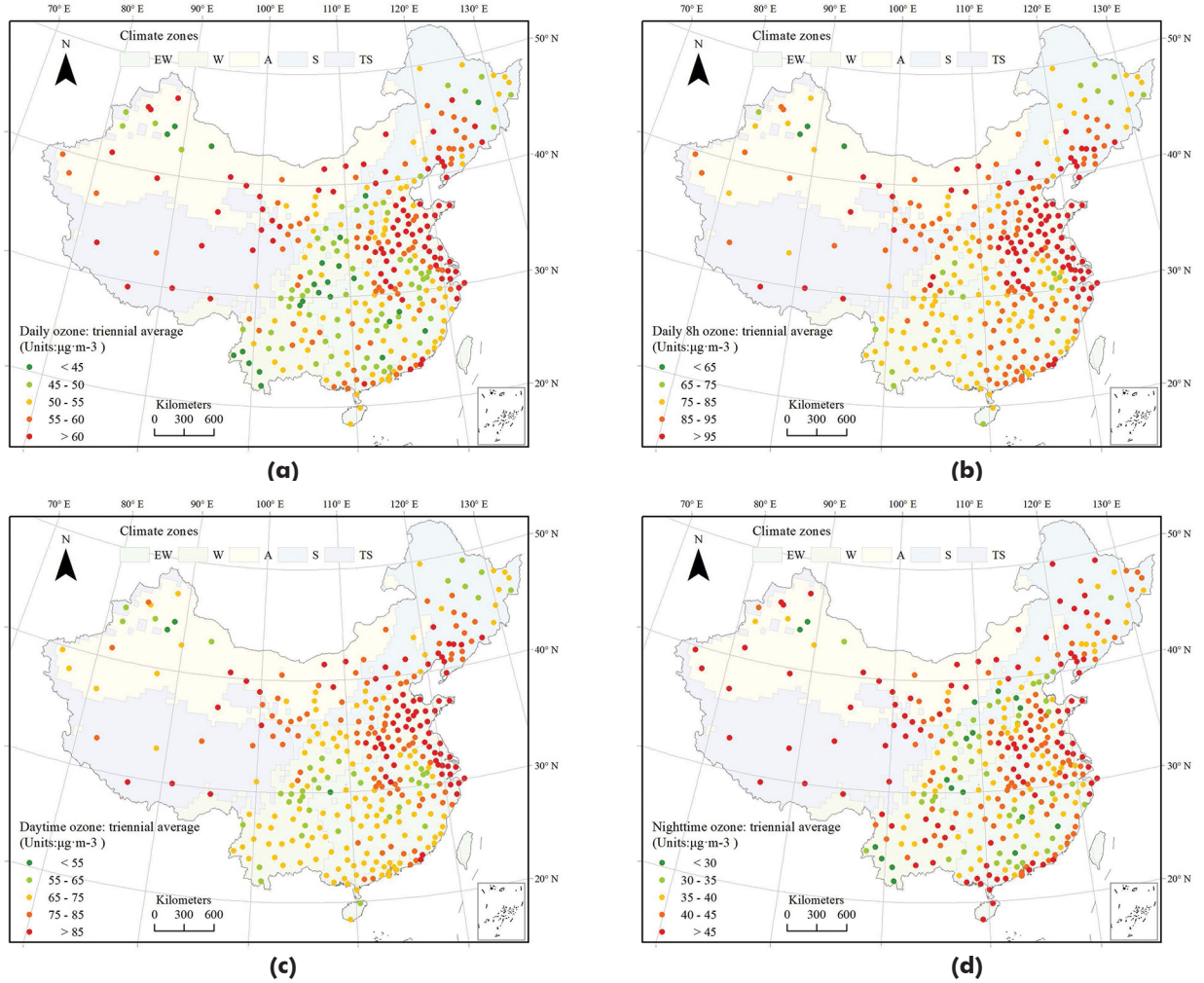

Figure 4. Triennial average PW concentrations of daily O_3, O_3-8h, daytime O_3, and nighttime O_3 for each urban area of the 339 cities. The shading color for each city relates to the climate zone.

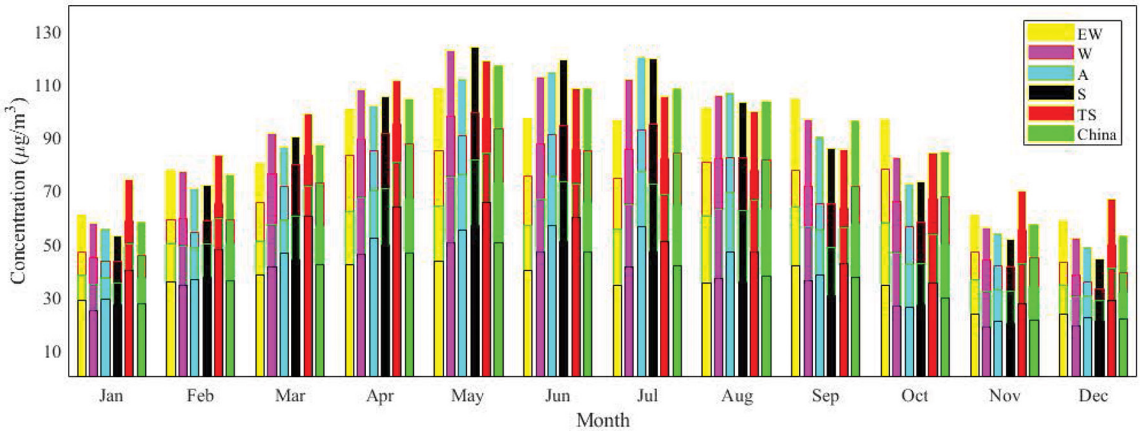

Figure 5. Monthly averages of the four ozone metrics in China for the five climate zones

season for each zone in this study is defined by this result. The exceedance rate during the ozone season (3.18%–11.32%) is approximately twice that of all the available days (1.04%–6.80%), and pollution in the W and EW zones is more frequent. For all the climate zones, the non-attainment days begin to sharply increase in April, and the most frequent ozone pollution occurs in May, while several of the urban areas in the S and TS climate zones still suffer from ozone pollution in July.

The Relationships Between Urban Ozone Pollution and Landscape Patterns

Spearman's rank correlation coefficients were applied to quantify the relationships between ozone concentrations during the ozone season and the urban landscape metrics across both climate zones and ozone formation regimes. According to the regime criteria (Table 3), the most polluted urban areas are located in the EW and W zones, while there are also 10 instances in the A zone and 33 instances in the S zone. As shown in Table 3, more than half the urban areas are assigned as precursor-controlled regions, most of which are located in the EW and W zones. The correlations for all the pollutant measurements are listed in Table 5, as represented by the O_3-8h results detailed below.

For the demographic distribution, only the polluted urban areas assigned as transitional regimes indicate some correlation to O_3-8h (Table 5). In detail, population in the EW region is moderately and positively associated with O_3-8h concentration ($r = 0.44$, $p < 0.05$). In addition, population heterogeneity (POPV) in the W climate zone facilitates the alleviation of O_3-8h concentration ($r = -0.40$, $p < 0.01$). In addition, the POPV in the NO_x-limited EW areas is positively associated with ozone concentration ($r = 0.29$, $p < 0.1$). With regard to physical layout, neither NO_x-limited areas nor transitional urban areas in the S zone present significant correlation. In detail, when ozone formation is controlled by both kinds of precursors, the total area is positively correlated to O_3-8h concentration in both the W ($r = 0.59$, $p < 0.01$) and EW ($r = 0.31$, $p < 0.05$) climate zones. In view of the spatial arrangement, the fragmentation level of built-up patches (NP) is positively associated with the O_3-8h concentration in all the zones (except for the S zone); the elongation level of urban areas (RCC) facilitates ozone dilution in the EW region ($r = -0.41$, $p < 0.05$); built-up continuity (LSI) is positively associated with the O_3-8h concentration in the EW and A zones ($r = 0.66$, $p < 0.001$ in the EW zone; $r = 0.75$, $p < 0.05$ in the A zone); and road density (RD) is proportional to the O_3-8h concentration in the EW zone ($r = 0.50$, $p < 0.05$). In addition, distance to coast (DIST) is strongly and positively associated with the O_3-8h concentration in all the urban areas (except for the S zone) during the ozone season. Meanwhile, the relationships in the national-scale analysis are consistent with those in the regional analysis, but the values are weaker.

Discussion

The rapid urbanization in China has focused public attention on both environmental protection and urban planning. Against a backdrop of rising ground-level ozone pollution, subject to the measurement limitations and the complicated chemical process, the ozone pollution situation of urban areas in China is still unclear. In this paper, we have analyzed the ozone concentration data collected from the newest national air quality monitoring network in 339 prefecture-level (or above) cities from June 2014 to May 2017. By reporting the situation of the PW ground-level ozone pollution in urban areas nationwide and describing the associations with urban characteristics, this research will help to expand our scientific understanding, and

Table 5. Spearman's rank correlation coefficients in the different ozone regimes between the O_3-8h during the ozone season and the urban landscape metrics across the climate zones and China as a whole

	Climate zone	EW		W		A	S		China	
Ozone metric	Regime	NOx-limited	Transitional	NOx-limited	Transitional	Transitional	NOx-limited	Transitional	NOx-limited	Transitional
	Num.	37	27	31	41	10	14	19	86	97
Daily	POPI	−0.15	0.31	0.24	0.19	−0.28	−0.07	0.24	0.12	0.18*
	POPV	0.08	−0.19	−0.07	**−0.33**[a]	−0.14	0.01	0.22	0.01	−0.16
	CA	−0.16	**0.42**[a]	0.33*	0.28*	−0.27	−0.02	0.30	**0.22**[a]	**0.29**[b]
	NP	0.16	**0.48**[a]	0.28	0.27*	−0.08	−0.16	−0.10	**0.25**[a]	**0.27**[b]
	LSI	0.05	**0.42**[a]	0.03	0.16	0.30	−0.20	−0.27	0.00	0.17*
	RCC	−0.17	−0.25	−0.12	−0.14	**0.78**[a]	0.26	−0.27	−0.15	−0.09
	DIST	−0.03	**−0.72**[d]	**−0.51**[b]	**−0.66**[d]	−0.15	−0.36	−0.23	**−0.35**[b]	**−0.44**[d]
	RD	0.08	**0.42**[a]	−0.17	−0.19	0.08	0.23	−0.15	−0.02	−0.03
Daytime	POPI	−0.09	0.34*	0.07	0.20	−0.13	−0.04	0.22	0.03	**0.23**[a]
	POPV	**0.38**[a]	−0.23	0.13	**−0.33**[a]	−0.31	0.11	0.29	0.20	−0.16
	CA	−0.21	**0.47**[a]	0.13	**0.33**[a]	0.01	−0.02	0.31	0.08	**0.37**[c]
	NP	0.04	**0.54**[b]	0.15	**0.32**[a]	0.27	−0.18	−0.05	0.14	**0.33**[c]
	LSI	−0.02	**0.51**[b]	−0.12	0.18	0.54	−0.17	−0.24	−0.13	**0.21**[a]
	RCC	−0.11	−0.30	−0.15	−0.13	0.49	0.19	−0.31	−0.16	−0.15
	DIST	0.30*	**−0.65**[c]	−0.17	**−0.69**[d]	−0.53	−0.49*	−0.34	−0.05	**−0.38**[c]
	RD	−0.10	0.38*	−0.21	−0.17	0.14	0.08	−0.19	−0.14	−0.07
Nighttime	POPI	−0.16	0.38	0.33	0.15	0.04	−0.34	0.21	0.13	**0.23**[a]
	POPV	0.01	−0.22	−0.12	**−0.43**[b]	−0.04	0.21	0.35	−0.02	**−0.21**[a]
	CA	−0.08	**0.52**[b]	**0.42**[a]	**0.31**[a]	0.08	−0.29	0.19	**0.25**[a]	**0.39**[d]
	NP	0.16	**0.59**[b]	**0.43**[a]	0.29	0.19	−0.21	−0.11	**0.30**[b]	**0.42**[d]
	LSI	−0.14	**0.55**[b]	0.13	0.19	0.54	−0.34	−0.25	−0.01	**0.31**[b]
	RCC	−0.05	−0.36	−0.27	−0.17	0.61	0.14	−0.27	−0.17	−0.18
	DIST	−0.06	**−0.69**[c]	**−0.45**[a]	**−0.72**[d]	−0.48	−0.37	−0.26	**−0.33**[b]	**−0.52**[d]
	RD	0.09	**0.44**[a]	−0.03	−0.24	0.02	0.24	−0.11	0.05	0.00
O_3-8h	POPI	−0.13	**0.44**[a]	0.21	0.15	0.19	−0.23	0.19	0.05	**0.28**[b]
	POPV	0.29*	−0.20	0.11	**−0.40**[b]	−0.31	0.16	0.38	0.18*	−0.19*
	CA	−0.18	**0.59**[b]	0.22	**0.31**[a]	0.35	−0.22	0.17	0.09	**0.44**[d]
	NP	0.01	**0.67**[c]	0.29	0.30*	0.58*	−0.27	−0.09	0.17	**0.46**[d]
	LSI	−0.16	**0.66**[c]	−0.03	0.16	**0.75**[a]	−0.34	−0.25	−0.12	**0.33**[c]
	RCC	0.03	**−0.41**[a]	−0.26	−0.15	0.16	0.09	−0.24	−0.17	**−0.21**[a]
	DIST	0.25	**−0.58**[b]	−0.10	**−0.74**[d]	**−0.93**[c]	−0.49*	−0.33	−0.04	**−0.47**[d]
	RD	−0.08	**0.50**[a]	−0.10	−0.21	0.30	0.04	−0.16	−0.07	−0.02

*significant at the 0.1 level (two-tailed) ; [a] significant at the 0.05 level (two-tailed); [b] significant at the 0.01 level (two-tailed); [c] significant at the 0.001 level (two-tailed); [d] significant at the 0.0001 level (two-tailed).

has important theoretical and management implications. To mitigate the impact of urban characteristics on ozone, urban planners will be able to gain insights into optimizing the spatial distribution of both demographic and physical layouts.

In contrast to the recent studies that have mainly focused on developed regions (Shao *et al.*, 2016; Shu *et al.*, 2016), this paper has reported on the ozone status in the urban areas of multiple cities. As an addition to the survey of ozone and the proportion of days violating the NAAQS standard (160 μg/m^3) of 15 typical cities in 2015 (Liu *et al.*, 2018), this research further reports on the most recent three-year situation in all the urban areas of China and the associated non-attainment rates. During the study period, the national triennial average was 88.68±10.41 μg/m^3 for O_3-8h, and around 5.27% of the days were non-attainment days that exceeded the new NAAQS standard of China. However, this rate is much lower than that reported in Liu *et al.*, (2018), as the typical cities in this previous study are metropolises located in heavily polluted regions (Figure 4). In addition, it is also demonstrated that the stringent guideline (i.e., 100 μg/m^3 for O_3-8h) is still hard to meet, as more than 30% of the days for each climate zone exceeded this standard between June 2014 to May 2017 (Table 4).

In view of the spatial distribution, the high ozone concentrations to the west of the Aihui-Tengchong Line are mainly due to natural activity (such as the strong UV and vertical transportation), while those in the EW and W climate zones are more closely associated with human activity (Table 3). In these zones, NCP, YRD, and PRD are pollution hot spots, and local industry and transportation are the dominant anthropogenic sources (Wang *et al.*, 2017). In view of the temporal distribution, the urban ozone concentrations show a remarkable seasonal and diurnal variability, which is strongly affected by the synoptic meteorological conditions (i.e., high temperature and stagnant weather). Overall, the spatio-temporal results suggest that specific control measures and mitigation strategies should be targeted in the different regions of China, in terms of the different features of local/regional emissions and meteorology.

The Spearman's rank bivariate correlation analysis was conducted by controlling the ozone sensitivity and weather conditions, and the associations with the spatial distribution of population and built-up land were investigated during the ozone season. Urban residents, who are not only the victims of pollution but also the source of the pollutant precursors, can be expected to have a great effect on urban ozone concentration. As the proportion of urban residents is expected to reach 70–80% by the year 2030, this effect is worthy of attention. At a certain level of population scale, large variation is often associated with resource inequity and suburban expansion, which can intensify air pollution in urban areas. As expected, in the EW climate zone, the ozone concentration shows a concomitant increase in population size for the transitional regime areas and heterogeneity (POPV) for the NO_x-limited urban areas. However, the negative relationship between POPV and ozone concentration for the transitional regime areas in the W climate zone is counterintuitive. A potential reason for this may be the large variation of population but modest population density (see POPI and population density (POPD) in Table 2) in this region.

At the same time, spatial patterns of emissions and pollutant concentrations can also be altered by city planning; for instance, the spatial distribution of built-up patches. Firstly, in the NO_x-limited regions, the insignificant correlations indicate that the contribution to pollution from anthropogenic VOC emissions (in the built environment) is minor. It is also noted that no urbanization-induced factor is associated with ozone pollution in the S zone, which is partly due to the limited sample size and the decrease of concentration with the increase of latitude (Figure 4). With regard to the precursor-controlled areas, increasing the total area of built-up land, urban sprawl in physical expansion, and built-up contiguity can lead to aggravation of the ozone concentration, which can be partly explained by increased vehicle exhaust emissions and fuel volatilization. In addition, the positive associations between DIST and ozone concentration suggest that the sea-land breeze acts as important meteorological assistance to distribute ozone in coastal cities, while the anticyclones and tropical cyclones in the western Pacific promote pollution production, recirculation, and accumulation. Several studies have noted this phenomenon in developed cities in both the YRD and PRD (Wang *et al.*, 2017), and we have further proved the existence nationwide. As the sea-land breeze can be intensified by the coastal urban heat island phenomenon (Li *et al.*, 2017), further attention to ozone and its precursors for the coastal cities is needed.

It is of interest to link the emerging theory of urban air environment protection and the management of urban landscapes, as it provides a new idea for stringent ozone pollution control measures. Encouraging residents to move out of urban areas has long been viewed as an effective way to mitigate ozone pollution. Essentially, large population variations can be mainly attributed to the uneven distribution of resources, as households vote with their feet to achieve a balance between the cost of living and local public goods. Many first-tier cities, such as Beijing, Shanghai, and Guangzhou, have established goals and implemented strategies to re-home millions of downtown residents. Our results should inspire a similar approach for the small cities. Meanwhile, with the private car annual growth rate at 22.76% in Chinese cities (Zheng and Kahn, 2013), this could further aggravate ozone pollution. In addition to fuel taxes, congestion tolls, vehicles with low emission, etc., planning the built-up environment to facilitate the dilution ability and reduce travel time could also be taken into consideration. The results from this study will provide additional evidence for promoting the management and implementation of related population policies and improving the urban ecology and air environment, particularly for locations where urbanization is still in process.

This study does have some limitations. The unbalanced spatial distribution of the *in-situ* stations and the inverse distance weighted interpolation suggested in previous studies (Clark *et al.*, 2011) may import some uncertainties into the estimation of the urban ozone concentration to the west of the Aihui-Tengchong Line. In addition, the population dataset was collected in 2010, which may also bring some uncertainty. Based on the monitoring in past decades, previous studies have analyzed long-term trends and the dynamic relationships between ozone and urbanization (Clark *et al.*, 2011; Stone, 2008) in developed nations, whereas the static ozone pollutant situation was addressed in this study. It is also noted that the most recent three-year average was utilized to avoid the specificity from a given year.

Conclusions

This paper has presented the ground-level ozone concentrations measured during three years of continuous monitoring in 339 prefecture-level cities in China between 2014 and 2017, and we have also described the relationships between human activity and ozone concentration in the most polluted cities. During the study period, the national triennial average was 55.34±7.77 μg/m^3 for daily ozone and 88.68±10.41 μg /m^3 for O_3-8h, and 5.27% of the days were non-attainment days that exceeded the new NAAQS standard (160 μg/m^3) of China. The urban ozone concentrations showed remarkable seasonal, diurnal, and spatial variability, which suggests that specific control measures and mitigation strategies should be targeted in the different regions of China, in terms of the different features of local/regional emissions and meteorology. It was found that both the spatial arrangement (including composition and configuration) of built-up areas and population density affect the concentration of ozone, which could provide us with important insights into the ecological design and management of urban areas. This

suggests that the impact of urbanization on ozone could be mitigated by balancing the spatial distribution of urban residents and optimizing the built-up area configuration in China.

Acknowledgements

The research was supported by the National Natural Science Foundation of China under Grants 41522110, 4176382 and 41771360, the National Program for Support of Top-notch Young Professionals, the Hubei Provincial Natural Science Foundation of China under Grant 2017CFA029, Hubei Provincial Natural Science Foundation Project under Grant 2017CFB188, , Open Fund of Ministry of Education key Laboratory under Grant 2016LSDMIS04, and the National Key R&D Program of China under Grant 2016YFB0501403 and 2017YFB0504103.

References

Bai, X., J. Chen, and P. Shi, 2011. Landscape urbanization and economic growth in China: Positive feedbacks and sustainability dilemmas, *Environmental Science & Technology*, 46(1):132-139.

Bechle, M.J., D.B. Millet, and J.D. Marshall, 2011. Effects of income and urban form on urban NO_2: Global evidence from satellites, *Environmental Science & Technology*, 45(11):4914-4919.

Guangdong Provincial Environmental Monitoring Center (GPEMC), 2017. Pearl River Delta Regional Air Quality Monitoring Network - A Report of Monitoring Results in 2016 (PRDAIR-2016-5).

Chinese MEP, 2012. Ambient air quality standards (GB 3095 2012) available at: URL: *Http://kjs.Mep.Gov.Cn/hjbhbz/bzwb/dqhjbh/dqhjzlbz/201203/w020120410330232398521.Pdf* (last date accessed: 02 January 2017).

Clark, L.P., D.B. Millet, and J.D. Marshall, 2011. Air quality and urban form in us urban areas: Evidence from regulatory monitors, *Environmental Science & Technology*, 45(16):7028-7035.

De Smedt, I., T. Stavrakou, F. Hendrick, T. Danckaert, T. Vlemmix, G. Pinardi, N. Theys, C. Lerot, C. Gielen, and C. Vigouroux, 2015. Diurnal, seasonal and long-term variations of global formaldehyde columns inferred from combined OMI and GOME-2 observations, *Atmospheric Chemistry & Physics Discussions*, 15(8).

Fang, C., G. Li, and S. Wang, 2016. Changing and differentiated urban landscape in China: Spatiotemporal patterns and driving forces, *Environmental Science & Technology*, 50(5):2217-2227.

Feng, Z., E. Hu, X. Wang, L. Jiang, and X. Liu, 2015. Ground-level O_3 pollution and its impacts on food crops in China: A review, *Environmental Pollution*, 199:42-48.

Frank, L.D., and P. Engelke, 2005. Multiple impacts of the built environment on public health: Walkable places and the exposure to air pollution, *International Regional Science Review*, 28(2):193-216.

Fu, J., D. Jiang, and Y. Huang, 2014. China grid population distribution data set (population grid_china), *Global Change Science Research Data Publishing System*.

Huang, J., C. Zhou, X. Lee, Y. Bao, X. Zhao, J. Fung, A. Richter, X. Liu, and Y. Zheng, 2013. The effects of rapid urbanization on the levels in tropospheric nitrogen dioxide and ozone over east China, *Atmospheric Environment*, 77:558-567.

Jia, C., X. Mao, T. Huang, X. Liang, Y. Wang, Y. Shen, W. Jiang, H. Wang, Z. Bai, and M. Ma, 2016. Non-methane hydrocarbons (NMHCs) and their contribution to ozone formation potential in a petrochemical industrialized city, northwest China, *Atmospheric Research*, 169:225-236.

Jin, X., A.M. Fiore, L.T. Murray, L.C. Valin, L.N. Lamsal, B. Duncan, K. Folkert Boersma, I. De Smedt, G.G. Abad, and K. Chance, 2017. Evaluating a space-based indicator of surface ozone-NOx-VOC sensitivity over midlatitude source regions and application to decadal trends, *Journal of Geophysical Research: Atmospheres*, 122(19).

Jin, X., and T. Holloway, 2015. Spatial and temporal variability of ozone sensitivity over China observed from the ozone monitoring instrument, *Journal of Geophysical Research: Atmospheres*, 120(14):7229-7246.

Larkin, A., A. van Donkelaar, J.A. Geddes, R.V. Martin, and P. Hystad, 2016. Relationships between changes in urban characteristics and air quality in east Asia from 2000 to 2010, *Environmental Science & Technology*, 50(17):9142-9149.

Lefohn, A.S., C.S. Malley, H. Simon, B. Wells, X. Xu, L. Zhang, and T. Wang, 2017. Responses of human health and vegetation exposure metrics to changes in ozone concentration distributions in the European Union, United States, and China, *Atmospheric Environment*, 152:123-145.

Lelieveld, J., J.S. Evans, M. Fnais, D. Giannadaki, and A. Pozzer, 2015. The contribution of outdoor air pollution sources to premature mortality on a global scale, *Nature*, 525(7569):367-371.

Li, G., C. Fang, S. Wang, and S. Sun, 2016. The effect of economic growth, urbanization, and industrialization on fine particulate matter (PM2.5) concentrations in China, *Environmental Science & Technology*, 50(21):11452-11459.

Li, M., T. Wang, M. Xie, B. Zhuang, S. Li, Y. Han, Y. Song, and N. Cheng, 2017. Improved meteorology and ozone air quality simulations using MODIS land surface parameters in the Yangtze river delta urban cluster, China, *Journal of Geophysical Research: Atmospheres*, 122(5):3116-3140.

Liu, C., P. Yin, R. Chen, X. Meng, L. Wang, Y. Niu, Z. Lin, Y. Liu, J. Liu, and J. Qi, 2018. Ambient carbon monoxide and cardiovascular mortality: A nationwide time-series analysis in 272 cities in China, *The Lancet Planetary Health*, 2(1):e12–e18.

Liu, H., S. Liu, B. Xue, Z. Lv, Z. Meng, X. Yang, T. Xue, Q. Yu, and K. He, 2018. Ground-level ozone pollution and its health impacts in China, *Atmospheric Environment*, 173:223-230.

Liu, J., W. Kuang, Z. Zhang, X. Xu, Y. Qin, J. Ning, W. Zhou, S. Zhang, R. Li, C. Yan, S. Wu, X. Shi, N. Jiang, D. Yu, X. Pan, and W. Chi, 2014. Spatiotemporal characteristics, patterns, and causes of land-use changes in China since the late 1980s, *Journal of Geographical Sciences*, 24(2):195-210.

McCarty, J., and N. Kaza, 2015. Urban form and air quality in the united states, *Landscape and Urban Planning*, 139:168-179.

Oke, T.R., 1982. The energetic basis of the urban heat island, *Quarterly Journal of the Royal Meteorological Society*, 108(455):1-24.

Ou, J., Z. Yuan, J. Zheng, Z. Huang, M. Shao, Z. Li, X. Huang, H. Guo, and P.K. Louie, 2016. Ambient ozone control in a photochemically active region: Short-term despiking or long-term attainment? *Environmental Science & Technology*, 50(11):5720-5728.

Pontius, J., and R. Gilmore, 2017. European landscape dynamics: Corine land cover data, *Photogrammetric Engineering & Remote Sensing*, 83(2):79-89.

Rubel, F., and M. Kottek, 2010. Observed and projected climate shifts 1901–2100 depicted by world maps of the Köppen-Geiger climate classification, *Meteorologische Zeitschrift*, 19(2):135-141.

Shao, P., J. An, J. Xin, F. Wu, J. Wang, D. Ji, and Y. Wang, 2016. Source apportionment of VOCs and the contribution to photochemical ozone formation during summer in the typical industrial area in the Yangtze river delta, China, *Atmospheric Research*, 176-177:64-74.

Shu, L., M. Xie, T. Wang, D. Gao, P. Chen, Y. Han, S. Li, B. Zhuang, and M. Li, 2016. Integrated studies of a regional ozone pollution synthetically affected by subtropical high and typhoon system in the Yangtze River delta region, China, *Atmospheric Chemistry and Physics*, 16(24):15801-15819.

Stone, B., 2008. Urban sprawl and air quality in large us cities, *Journal of Environmental Management*, 86(4):688-698.

Wang, T., L. Xue, P. Brimblecombe, Y.F. Lam, L. Li, and L. Zhang, 2017. Ozone pollution in China: A review of concentrations, meteorological influences, chemical precursors, and effects, *Science of the Total environment*, 575(Supplement C):1582-1596.

Zheng, S., and M.E. Kahn, 2013. Understanding China's urban pollution dynamics, *Journal of Economic Literature*, 51(3):731-772.

Zhu, H., Y. Li, Z. Liu, and B. Fu, 2015. Estimating the population distribution in a county area in China based on impervious surfaces, *Photogrammetric Engineering & Remote Sensing*, 81(2):155-163.

Ziemke, J.R., S. Chandra, B.N. Duncan, L. Froidevaux, P.K. Bhartia, P.F. Levelt, and J.W. Waters, 2006. Tropospheric ozone determined from aura OMI and MLS: Evaluation of measurements and comparison with the global modeling initiative's chemical transport model, *Journal of Geophysical Research: Atmospheres*, 111(D19).

Zou, X., Z. Shen, T. Yuan, S. Yin, X. Zhang, R. Yin, P. Zhou, and W. Wang, 2007. On an empirical relationship between SO_2 concentration and distance from a highway using passive samplers: A case study in Shanghai, China, *Science of the Total Environment*, 377(2):434-438.